FUDMA Journal of Sciences (FJS)
ISSN online: 2616-1370
ISSN print: 2645 - 2944
Vol. 9 No. 1, January, 2025, pp 258 - 264
DOI: https://doi.org/10.33003/fjs-2025-0901-3178

EFFICACIES OF CORROSION INHIBITION ABILITY OF SYNTHESIZED CUO NANOPARTICLES OF *JATROPHA TANJORENSIS* AND *PRUNUS DOMESTICA* LEAVES EXTRACTS ON MILD STEEL IN ACIDIC MEDIUM

[1]Garba, S., [1]Tanko, S. A., *[1]Mathew, J., [1]Nwaedozie, J. M., [2]Agbogo, U. V. and [1]Rifore, B. S.

[1]Nigerian Defence Academy, Department of Chemistry, Kaduna
[2]Nigerian Army University, Department of Chemistry, Biu

*Corresponding authors' email: jojomathew2222@gmail.com

ABSTRACT

Corrosion inhibitions of mild steel in sulphuric acid medium by CuO nanoparticle of Jatropha tanjorensis extract (CuO NPs –JT) and CuO nanoparticle of Prunus domestica extract (CuO NPs –PD) were studied by weight loss method. The influence of extract concentrations (0.4g/l to 1.6g/l) and temperatures (303K to 333K) on mild steel corrosion and corrosion inhibition were assessed. The corrosion rate decreased with increasing CuO nanoparticles concentration for mild steel at 303 K. Inhibition efficiency in all the systems decreased with a rise in temperature, suggesting physical adsorption of the nanoparticles constituents on the metal surfaces in both CuO NPs –JT and CuO NPs –PD. The highest inhibition efficiency of 88.1% occurred at CuO NPs – JT concentration of 1.6 g/L at 30°C and 93.4% occurred at CuO NPs – PD concentration of 1.6g/l at 30°C.The results of the studies showed that CuO NPs – PD exhibited the highest inhibition efficiency at different temperature and concentration of inhibitors then that of CuO NPs – JT on the surface of mild steel metal in an acidic medium. The results obtained showed that the CuO nanoparticles decreased the corrosion rate of mild steel in the acid medium. The calculated thermodynamic parameters indicate that the adsorption process was endothermic and spontaneous and the negative values of $\Delta S°_{ads}$ indicate a decrease in the disorderliness of the adsorption process. Corrosion activation energy (E_a) values for mild steel in the acid solutions increased in the presence of the CuO nanoparticles inhibitor and were found to be less than 80 kJmol^{-1}.

Keywords: Corrosion, Nanoparticles, Inhibitors, Thermodynamic, Adsorption, *Jatropha tanjorensis*, *Prunus domestica*

INTRODUCTION

Since companies use so many different kinds of materials, corrosion has become a hot topic as of late. Chemical plant leaks, decreased equipment efficiency, shorter life length, and higher exposure to damage and dangers are all attributed to it (Kristy *et al.*, 2021). Both safety issues and financial losses may be caused by corrosion. Dariva and Galio (2014) cite research from the National Association of Corrosion Engineers (NACE) that estimates the worldwide damage caused by corrosion to be roughly US$2.5 trillion, or around 3.4% of global GDP. Unless more sophisticated methods of controlling corrosion are discovered, this expense is projected to increase every year. A portion of these costs are often paid for out of pocket. Some examples of direct expenses include the following: storage, repair, and replacement of corroded metal components; plating, galvanization, and metal and alloy modification; and losses from the fabrication and use of corrosion inhibitors. Coatings, transportation pipeline leaks, contaminated liquids, and the cost to clean them all contribute to corrosion's indirect cost (Koch, 2017). The direct and indirect costs of corrosion damage are usually considered to be equal in every case; together, they amount to 3.4% of world GDP.A more chemically stable oxide is produced by the natural process of corrosion, which transforms a refined metal. Exposure to environmental chemicals or electrochemical reactions causes materials (often metals) to corrode over time (Honarvar *et al*., 2020).The oxidation or loss of electrons due to degradation of the material's atoms is another way to define corrosion. As soon as there is a enough amount of oxygen and moisture, the equipment begins to corrode. Chemical species like acids, bases, and salts usually speed up this process (Kristy *et al*., 2021).Controlling and preventing corrosion is the focus of corrosion engineering. In most cases, the process involves an oxidant like oxygen, hydrogen, or hydroxide reacting with a metal by electrochemical oxidation. As an example of electrochemical corrosion, rusting is a well-known process that forms iron oxides. Iron oxidation increases and electron loss occurs during rusting. There are primarily two types of iron oxides that make up rust (Honarvar *et al*., 2020). The following chemical processes cause iron to rust:

$$2Fe(s) \rightarrow 2Fe^{2+}(aq) + 4e^{-} \quad (1.1)$$

$$4e^{-} + 4H^{+}(aq) + O_2(g) \rightarrow 2H_2O \quad (1.2)$$

$$2Fe(s) + 4H^{+}(aq) + O_2(g) \rightarrow 2Fe^{2+}(aq) + 2H_2O \quad (1.3)$$

$$4Fe(s) + O_2(g) + 7H_2O(l) \rightarrow 2Fe_2O_3.\frac{3}{2}H_2(\mathrm{s}) + 8H^{+}(aq) \quad (1.4)$$

As a consequence, metal rusting is a corrosive phenomenon. This form of damage generally creates oxides or salts of the original metal and resulting in a characteristic orange coloring. Corrosion may also occur in materials other than metals, such as ceramics or polymers, but in this context, the word 'degradation'' is more generally used (Fawzy *et al*., 2021). Mild steel is commonly utilized for plant structures such as storage tanks, pipelines, and reactors. In the process, petrochemical, oil and gas industries make use of it owing to its good mechanical qualities, but the slow loss of the metallic structures by corrosion attack, notably during pickling and acidization (Nayak *et al*., 2016), is a severe setback. The use of corrosion inhibitors is an effective technique of preventing mild steel corrosion consequently, nanoparticles have found useful uses in this field. Metal or metal oxide nanoparticles, both stand-alone and coupled with organic polymers to generate nanocomposites (Habib *et al*., 2021), which have been employed either as surface coatings or as additives used for acidic solutions to minimize metal corrosion degradation

MATERIALS AND METHODS

Sample Collection and Preparation

Fresh leaves of *Jatropha tanjurensis* and *Prunus domestica* were obtained from Sabon Tasha, Chikun local government, Kaduna State. The leaves of the plant samples were identified at the Herbarium unit of the Department of Biological Sciences, NDA with voucher number 25 and 26 respectively. The leaves were cleaned to remove dirt, dried at room temperature, mashed using a mortar and pestle and bagged for subsequent use.

Preparation of Leaf Extract

The fine powdered leaves (10 g) of J.T and P.D were measured into in a 250 cm3 beaker, mixed with 100 cm3 of deionized water and boiled at 80°C for 20 min. The mixture was filtered into another beaker using Whatman no.1 filter paper (Mathew *et al*., 2024) . The extracts were allowed to cool down and kept in the refrigerator (4°C) for usage of the nanoparticle

Preparation of Copper oxide Nanoparticles

For the synthesis of CuO NPs, 50 cm^3 of 0.05M aqueous solution of $CuSO_4.5H_2O$ (precursor) was combined with 8 cm3 of the produced aqueous leaf extract in a 500 cm^3 beaker. The pH of the mixture was adjusted to 12 by the drop-wise addition of 0.02 M aqueous NaOH solution.

The production of light blue particles showed the creation of CuO nanoparticles after the solution was agitated for 20 minutes with a magnetic stirrer at room temperature and allowed to settle. The supernatant solution was decanted and the residues were dried at room temperature for 48hours. The particles were calcined at 250-300°C for 1 h in a muffle furnace. The dark green powder produced were collected in a tiny sample vial after cooling and kept in a desiccator for subsequent use.

Weight Loss Method

The coupons were immersed in 100 cm^3 of 1.0 M H_2SO_4 in a beaker and extracted at three-hour intervals. The extracted coupon was moistened with distilled water, degreased with acetone, enveloped in filter paper, and positioned in a desiccator to facilitate drying. It was weighed promptly after desiccation. The coupon was then immersed in an acidic solution, with inhibitor concentrations adjusted to 0.4g, 0.8g, 1.2g, and 1.6g at temperatures of 30℃, 40℃, and 50℃, respectively (Awe *et al*., 2019).

The weight loss, corrosion rate, inhibition efficiency and surface coverage were calculated using the following equations: 2.1, 2.2, 2.3 and 2.4.

$$\Delta w = w_2 - w_1 \quad (2.1)$$

$$IE\% = \left(\frac{CRo - CR1}{CR1}\right) \times 100 \quad (2.2)$$

$$CR = \frac{\Delta w}{AT} \quad (2.3)$$

$$\Theta = \frac{\%IE}{100} \quad (2.4)$$

Where Δw is the weight loss, W_1 and W_2 are the weight before and weight after in grams, A is the area of the coupon, T is the total time of immersion in hours, CR is the corrosion rate in gcm^2h^{-1} while Θ is the surface coverage , IE is the inhibition efficiency , CR_O and CR_1 are corrosion rate of the mild steel coupon in the absence of inhibitor and corrosion rate of the mild steel coupon in the presence of inhibitor.

Determination of Activation Energy

The activation energy parameter of the corrosion inhibition process on mild steel surface were obtained using (Awe *et al*., 2015): equation 2.4.

$$\ln CR = -\left(\frac{E_a}{R}\right)\left(\frac{1}{T}\right) + \ln A \quad (2.5)$$

Where: CR is the rate of corrosion, Ea is the apparent activation energy, R is the universal gas constant, T is the absolute temperature, and A is the frequency factor.

Determination of Thermodynamic Parameters

The thermodynamic parameters such as enthalpy, and entropy of carbon steel corrosion inhibition in acidic medium was calculated using equation 2.5 (Mouheddin *et al*., 2018; Ogoke *et al*., 2009).

$$ln\ \frac{CR}{T} = [\ ln\frac{R}{Nh} + \frac{\Delta S_{ads}}{R}] - \frac{\Delta H_{ads}}{RT} \quad (2.6)$$

Where: h is the Planck's constant (6.626176×10^{-34} Js), N is the Avogadro's number,($6.022\times10^{23} mol^{-1}$), R is the Universal gas constant (8.314 J/Kmol) and T is the temperature of the medium.

RESULTS AND DISCUSSION

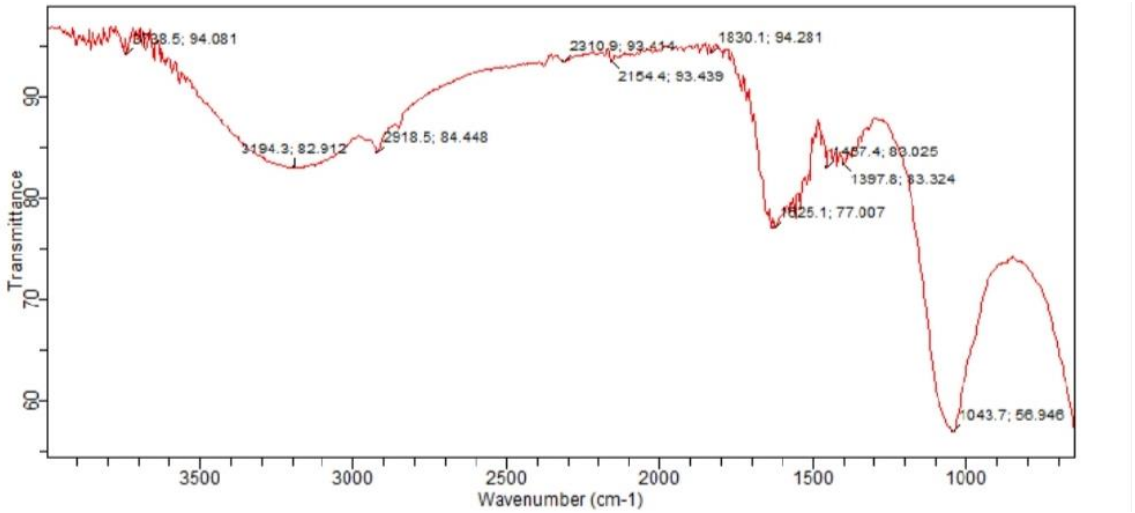

Figure 1: FTIR spectrum of CuO NPs – JT

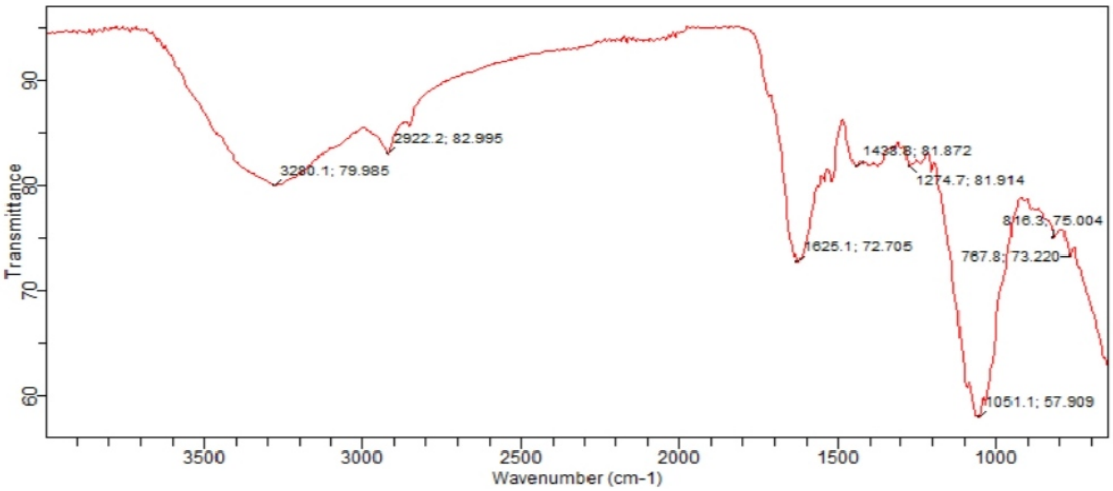

Figure 2: FTIR spectrum of CuO NPs – PD

The FTIR spectra of CuO NPs – JT and CuO -PD, recorded between 4000 cm^{-1} and 650 cm^{-1}, are shown in Fig. 1 and Fig. 2. For CuO NPs -JT, a large absorption band at 3280 cm^{-1} is attributed to the presence of -OH stretching vibrations. The peaks at 1625 cm^{-1} and 1397 cm^{-1} correspond to the asymmetric and symmetric vibrations of O–C–O, respectively. In the CuO NPs – JT spectrum, two distinct distinctive peaks at 1051 cm^{-1} correspond to the Cu-O-C bond from CuO. The FTIR spectrum data (Fig. 1) demonstrate that the carboxyl group combined with the hydroxyl group to effectively generate CuO nanoparticles throughout the reaction process (Li *et al.*, 2013). The FTIR analysis demonstrates strong alignment with the findings of Gao *et al.* (2016).In the FTIR spectrum of CuO NPs - PD, a wide peak at 3280 cm^{-1} corresponds to OH stretching vibrations, suggesting the presence of hydroxyl groups. The increased strength of the OH vibrations is due to the abundance of OH groups in the plant extract. A secondary peak at 1625 cm^{-1} is attributed to the vibrations of C=O and C=C, respectively. The peaks at 1397 cm^{-1} and 1051 cm^{-1} correspond to the C-OH stretching and O-H bending vibrations, respectively.

Table 1: Weight loss result of mild steel coupon in 1M H_2SO_4 in the presence of CuO nanoparticles synthesized using *Jatropha tanjorensis* leaves extract (CuO NPs – JT).

T (K)	Conc. (g/l) CuO NP-JT	Weight Loss (g)	CR (g/cm^2hr)	IE%	Θ
	Blank	0.02746	0.00071		
303K	0.4	0.01349	0.00035	50.9	0.509
	0.8	0.00893	0.00023	67.5	0.675
	1.2	0.00582	0.00015	78.8	0.788
	1.6	0.00328	0.0000844	88.1	0.881
313K	Blank	0.03948	0.00102		
	0.4	0.02411	0.00062	38.9	0.389
	0.8	0.01952	0.00050	50.6	0.506
	1.2	0.00854	0.00023	57.5	0.575
	1.6	0.005431	0.00014	72.2	0.722
323K	Blank	0.05823	0.00150		
	0.4	0.046115	0.00119	20.8	0.208
	0.8	0.03472	0.00089	40.4	0.404
	1.2	0.02987	0.00077	48.7	0.487
	1.6	0.01963	0.00051	66.2	0.662
333K	Blank	0.07945	0.00204		
	0.4	0.0668	0.00172	15.9	0.159
	0.8	0.05182	0.00133	34.8	0.348
	1.2	0.04943	0.00127	37.8	0.378
	1.6	0.03502	0.00090	55.9	0.559

Table 2: Weight loss result of mild steel coupon in 1M H_2SO_4 in the presence of CuO nanoparticles synthesized using Prunus *domestica* leaves extract (CuO NPs – PD)

T (K)	Conc. (g/l) CuO NP- PD	Weight Loss (g)	CR (g/cm^2hr)	IE%	Θ
	Blank	0.02444	0.000629		
303K	0.4	0.0114	0.000293	53.3	0.533
	0.8	0.00647	0.000166	73.5	0.735
	1.2	0.00439	0.000113	82	0.82
	1.6	0.0016	0.000041	93.4	0.934

313K	Blank	0.04281	0.001102		
	0.4	0.02226	0.000573	48	0.48
	0.8	0.01423	0.000366	66.7	0.667
	1.2	0.00995	0.000256	76.8	0.768
	1.6	0.00491	0.000126	88.5	0.885
323K	Blank	0.05701	0.001467		
	0.4	0.04011	0.001032	29.6	0.296
	0.8	0.02781	0.000716	51.2	0.512
	1.2	0.02227	0.000573	60.9	0.609
	1.6	0.00991	0.000255	82.6	0.826
333K	Blank	0.07214	0.001856		
	0.4	0.05481	0.00141	24	0.24
	0.8	0.04863	0.001251	32.5	0.325
	1.2	0.03452	0.000888	52.1	0.521
	1.6	0.01764	0.000454	75.5	0.755

Tables 1 and 2 from the weight loss experiment revealed that an increase in the concentration of both nanoparticles enhanced surface covering and inhibitory efficiency while concurrently reducing the corrosion rate. This is corroborated by the observation that an elevation in the inhibitor's concentration increased the quantity of active sites adsorbed on the metal surface. Consequently, the blank solution exhibited an elevated corrosion rate at 303K, 313K, 323K, and 333K, respectively. Furthermore, at all temperatures, 1.6g of each inhibitor had the greatest inhibition effectiveness at 3-hour intervals. The greatest inhibition efficiency (IE) for 1.6g of CuO nanoparticles – JT at 303K was 88.1%, while 1.6g of CuO nanoparticles – PD achieved a maximum IE of 93.4%. At 313 K, the inhibition effectiveness of both inhibitors decreased to 72.2% and 88.5%, while at 323 K, the inhibition efficiency of both inhibitors further declined to 66.2% and 82.6%. At a maximum temperature of 333K, the lowest inhibition efficiency was recorded at 0.4g of inhibitors. The inhibition efficiency was seen to rise with an increase in temperature. An increase in inhibition effectiveness with rising temperature suggests that both CuO NPs –JT and CuO NPs – PD functioned more effectively as inhibitors at elevated temperatures compared to lower temperatures. Moreover, the enhancement of inhibition efficacy with rising temperature suggests that the inhibitor chemically adsorbs onto the mild steel surface.

Activation Energy

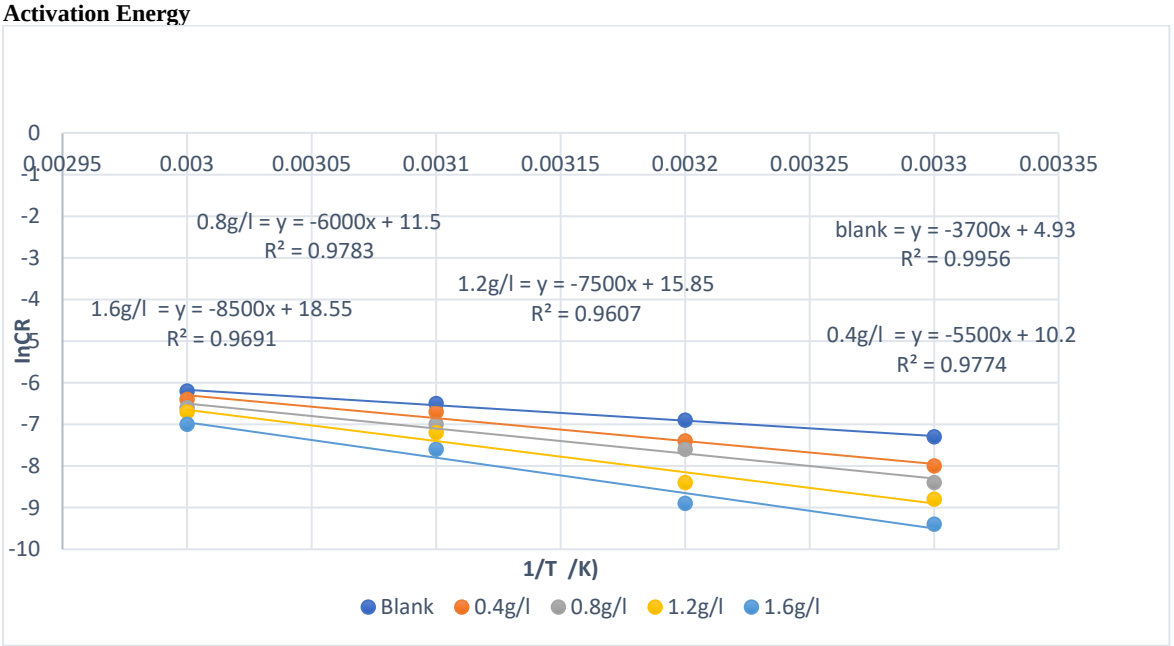

Figure 3: Arrhenius plots for the corrosion of mild steel in 1M H_2SO_4 in the absence and presence of CuO nanoparticles synthesized using *Jatropha tanjorensis* leaves extract (CuO NPs – JT)

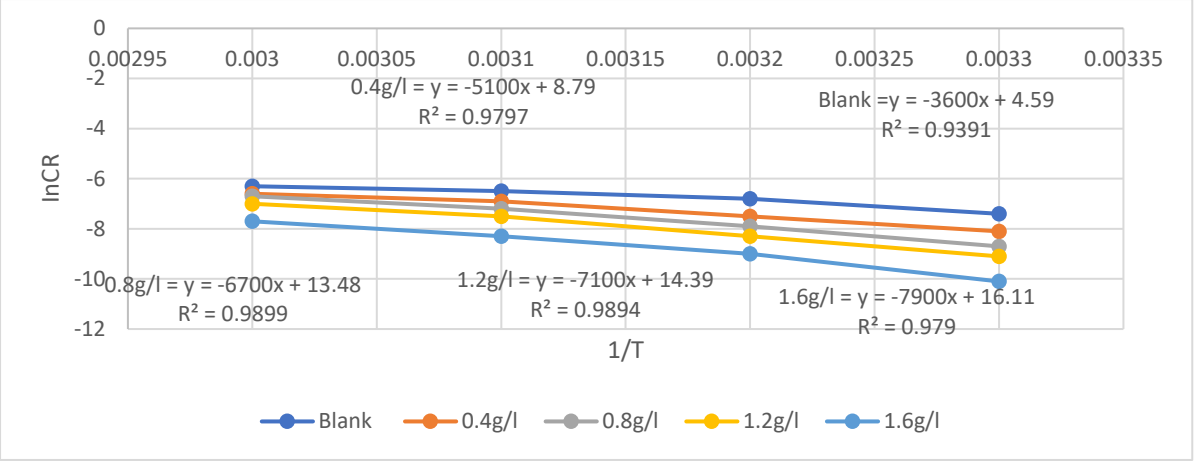

Figure 4: Arrhenius plots for the corrosion of mild steel in 1M H_2SO_4 in the absence and presence of CuO nanoparticles synthesized using Prunus *domestica* leaves extract (CuO NPs – PD)

Table 3: Arrhenius parameters for the adsorption of CuO NPs – JT on mild steel surface

System	Slope	InA	Ea (kJ/mol)		R^2
Blank	-3700	4.93	30.7618	138.3795123	0.9956
0.4g/l	-5500	10.2	45.727	26903.18607	0.9774
0.8g/l	-6000	11.5	49.884	98715.77101	0.9783
1.2g/l	-7500	15.85	62.355	7648346.204	0.9607
1.6g/l	-8500	18.55	70.669	113805339.7	0.9691

Table 4: Arrhenius parameters for the adsorption of CuO NPs – PD on mild steel surface

System	Slope	InA	Ea (kJ/mol)	A	R^2
Blank	-3600	4.59	29.9304	98.49443016	0.9391
0.4g/l	-5100	8.79	42.4014	6568.232175	0.9797
0.8g/l	-6700	13.48	55.7038	714972.958	0.9899
1.2g/l	-7100	14.39	59.0294	1776223.43	0.9894
1.6g/l	-7900	16.11	65.6806	9919370.306	0.979

The Ea values shown in Tables 3 and 4 were derived from the slopes of lnCR against 1/T graphs in Figures 3 and 4.The activation energy (Ea) values recorded for CuO nanoparticles – JT and CuO nanoparticles – PD exceeded the Ea value of the control, measuring 30.76 and 29.93 $kJmol^{-1}$, respectively. The activation energies were shown to rise with the concentration of nanoparticles, indicating a corresponding increase in adsorption strength with increasing concentration (Awe et *al*., 2017). Reduced Ea values seen with nanoparticles relative to the blank are ascribed to a physisorption mechanism, while the opposite suggests a chemisorption mechanism (Abakedi *et al*., 2017). It may be hypothesized that the adsorption of both CuO NPs – JT and CuO NPs -PD onto the mild steel surface happened via a chemisorption mechanism.

Investigation of Thermodynamics and Adsorption

In corrosion research, thermodynamic factors are helpful in forecasting the characteristics of adsorption, the viability of the adsorption process, and the thermal energy associated with adsorption.

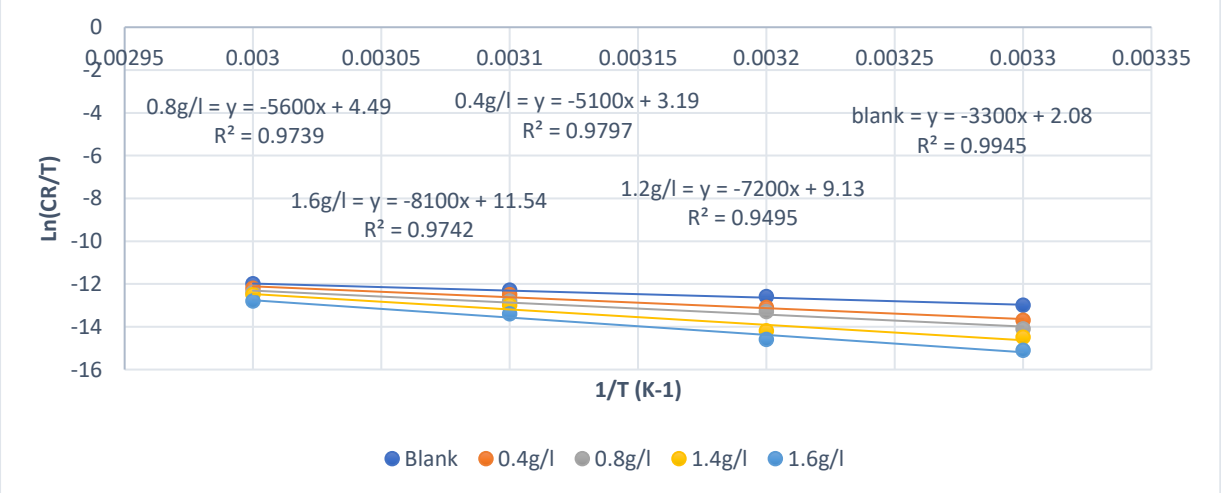

Figure 5: Transition state plot for mild steel corrosion in 1 M H_2SO_4 solution in the absence and presence of CuO NPs – J

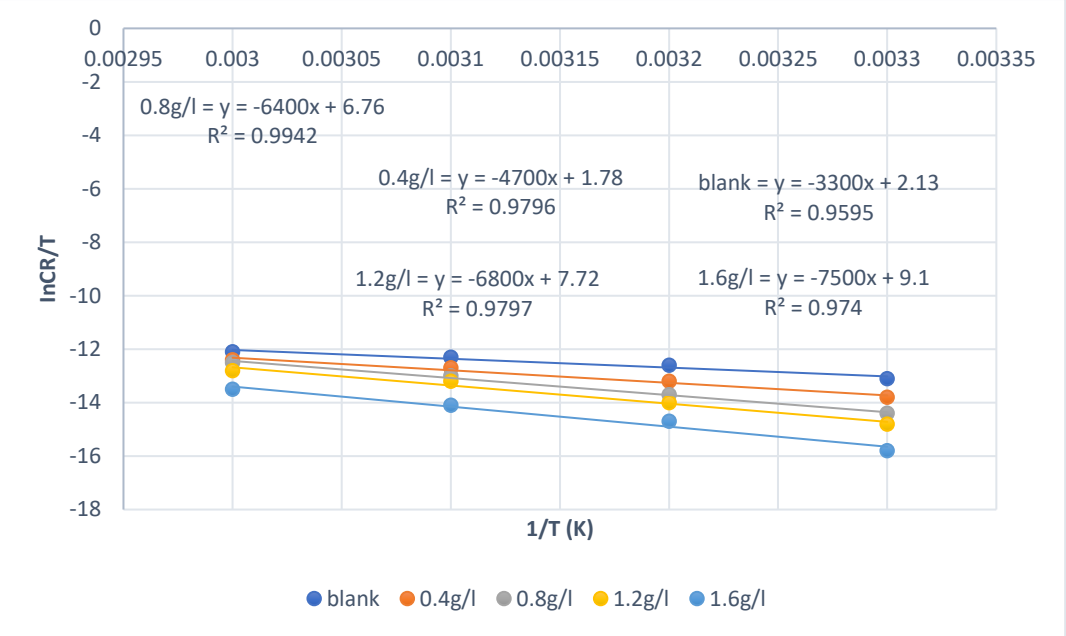

Figure 6: Transition state plot for mild steel corrosion in 1 M H_2SO_4 solution in the absence and presence of CuO NPs – PD

Table 5: Thermodynamic parameters for mild steel corrosion in 1 M H_2SO_4 solution in the absence and presence of CuO nanoparticles synthesized using *Jatropha tanjorensis* leaves extract (CuO NPs – JT)

CuO NPs – JT concentration	Slope	Intercept	ΔH_{ads} (KJ/mol)	ΔS_{ads} (J k^{-1} mol^{-1})	R^2
1M H_2SO_4 (Blank)	-3300	2.08	27.4362	-180.24752	0.9945
0.4g/l	-5100	3.19	42.4014	-171.01898	0.9797
0.8g/l	-5600	4.49	46.5584	-160.21078	0.9739
1.3g/l	-7200	9.13	59.8608	-121.63382	0.9495
1.6 g/l	-8100	11.54	67.3434	-101.59708	0.9742

Table 6: Thermodynamic parameters for mild steel corrosion in 1 M H_2SO_4 solution in the absence and presence of CuO nanoparticles synthesized using *Prunus Domestica* leaves extract (CuO NPs – PD)

CuO NPs – PD concentration	Slope	Intercept	ΔH_{ads} (kJ/mol)	ΔS_{ads} (J k^{-1} mol^{-1})	R^2
1M H_2SO_4 (Blank)	-3300	2.13	27.4362	-179.83182	0.9595
0.4g/l	-4700	1.78	39.0758	-182.74172	0.9796
0.8g/l	-6400	6.76	53.2096	-141.338	0.9942
1.3g/l	-6800	7.72	56.5352	-133.35656	0.9797
1.6 g/l	-7500	9.1	62.355	-121.88324	0.974

Values of $\Delta H°_{ads}$ and $\Delta S°_{ads}$ were calculated from the gradients ($-\Delta H°_{ads}/R$) and the intercepts [ln (R/Nh) + $\Delta S°_{ads}/R$] of ln (CR/T) vs. 1/T plots (Figs. 5 and 6), respectively, and presented in Table 5 and 6. The positive values of $\Delta H°_{ads}$ obtained reflect the endothermic nature of the corrosion inhibition process in the absence and presence of the CuO nanoparticles. The values of $\Delta S°_{ads}$ presented in Table 5 and 6 were negative. The negative values of $\Delta S°_{ads}$ indicate a decrease in the disorderliness of the adsorption process (Abakedi *et al*., 2016). In other words, the nanoparticles adhered strongly on the mild steel surface.

CONCLUSION

The comparative analysis of the corrosion inhibitive ability of CuO NPs –JT and CuO NPs - PD nanoparticles on mild steel was studied. The green synthesis of the various nanoparticles showed color changes which marked the successful reduction of the oxides to their nanosizes.Both nanoparticles were tested for their corrosion inhibition tendencies on mild steel in 1.0M sulphuric acid medium. They were tested at 303K, 313K, 323K and 333K respectively, while varying their concentrations at 0.4g/L, 0.8g/L , 1.2g/L and 1.6g/L respectively. It was discovered that both inhibitors decrease the corrosion rate as their concentration increased yielding a high inhibition efficiency of 88.1 % and 93.4% for CuO NPs –JT and CuO NPs - PD respectively. Therefore, from the results, CuO NPs-PD showed a higher inhibitor efficiency than that of CuO NPs –JT.The calculated thermodynamic parameters indicate that the adsorption process was endothermic and spontaneous. The negative values of $\Delta S°_{ads}$ indicate a decrease in the disorderliness of the adsorption process. Corrosion activation energy (E_a) values for mild steel in the acid solutions increased in the presence of the CuO nanoparticles inhibitor and were found to be less than 80 $kJmol^{-1}$.

REFERENCES

Awe, F. E., Idris, S. O. & Abdulwahab, M. (2016). Studies on the inhibitive properties of Boscia senegalensis in aluminium-HCl environment. Moroccan Journal of Chemistry, 4, pp. 629-638.

Awe, F. E., Idris, S. O., Abdulwahab, M. & Oguzie, E. E.(2015). Inhibitive and adsorptive effect of Parinari polyandra on mild steel corrosion in aqueous sulphuric acid. African Journal of Pure and Applied Chemistry, 9,6, pp. 125-134,.

Awe, F. E., M Abdulwahab & H. A. Otaru. (2019). Adsorptive studies of the inhibitive properties of ethanolic extracts of Parinari polyandra on Mild steel in acidic media.Communication in Physical Sciences journal. 4(1): 39-47.

Dariva, C., Galio, F., (2014). Corrosion Inhibitors – Principles, Mechanisms and Applications, InTech. 365-379.

Dariva, C.G., and Galio, A.F., (2014), "Corrosion Inhibitors – Principles, Mechanisms and Applications" in *Developments in Corrosion Protection*, Eds. Aliofkhazraei, M., IntechOpen, Rijeka, Croatia, 365–379.

De Damborenea, J., Conde, A., Arenas, M., (2014). Corrosion inhibition with rare earth metal compounds in aqueous solutions, Rare Earth-based Corrosion Inhibitors, Elsevier, 84–116. Search PubMed.

Eddy, N. O., Momoh-Yahaya, H. & Oguzie, E. E.(2015). Theoretical and experimental studies on the corrosion inhibition potentials of some purines for aluminum in 0.1 M HCl. Journal of Advanced Research 6, pp. 203-216.

Fawzy, A.; El-Sayed, R.; Al Bahir, A.; Morad, M.; Althagafi, I.; Althagafy, K (2021). Assessment of new designed surfactants as eco-friendly inhibitors for the corrosion of steel in acidic environment and evaluation of their biological and surface features: Thermodynamic, kinetic and mechanistic aspects. J. Adhes. Sci. Technol., pp1–27.

Honarvar Nazari, M.; Shihab, M.S.; Havens, E.A.; Shi, X (2020). Mechanism of corrosion protection in chloride solution by an apple-based green inhibitor: Experimental and theoretical studies. J. Infrastruct. Preserv. Resil., 1, pp1–19.

Hossain, N.; Iqbal, A.P.; Saha, T (2020). Colocasia Esculenta as a Corrosion Inhibitor in Low Si Containing Al-S Aluminum Alloy in HCL Colocasia Esculenta as a Corrosion Inhibitor in Low Si Containing Al-S Aluminum Alloy in HCL. J. Mech. Mech. Eng. ,6.

Koch, G., (2017). Cost of corrosion, Trends in oil and gas corrosion research and technologies, Elsevier 3–30.
Kristy, P., Cherfan, T., Asmar, J. (2021). Corrosion of the metals, effect of corrosion on different types of metals, Exp. Find. 1-3.

Mathew C.E., Valentine C.U., & Msenhenba M.M. (2024). Corrosion inhibitory of mixture of mixture of codiaum variegatum and ficus benjamina for mild steel in hydrochloric acid medium. FUDMA Journal of Science (FJS).8(5) pp 258–263. https://doi.org/10.33003/fjs-2024-0805-2677

Solomon, M. M.; Gerengi, H.; Kaya, T.; Umoren, S. A. (2017). Enhanced corrosion inhibition effect of chitosan for St37 in 15% H2SO4 environment by silver nanoparticles. Int. J. Biol. Macromol, 104, 638−649.

Solomon, M. M.; Gerengi, H.; Umoren, S. A. (2017). Carboxymethyl cellulose/silver nanoparticles composite: synthesis, characterization and application as a benign corrosion inhibitor for St37 steel in 15% H_2SO_4 medium. ACS Appl. Mater. Interfaces, 9, 6376−6389.

Solomon, M. M.; Umoren, S. A. (2015). Performance assessment of poly (methacrylic acid)/silver nanoparticles composite as corrosion inhibitor for aluminium in acidic environment. J. Adhes. Sci. Technol, 29, 2311−2333.